SEISMIC BEHAVIOR OF BRIDGE WITH PIER AND FOUNDATION STRENGTHENING USING PSEUDO-DYNAMIC TEST

Anawat CHOTESUWAN [1)], Hiroshi MUTSUYOSHI [1)] and Takeshi MAKI [1)]
[1)] Structural Material Lab., Department of Civil and Environmental Engineering, Saitama University

ABSTRACT

This paper describes the seismic behavior of reinforced concrete (RC) bridge piers and foundations based on pseudo-dynamic (PSD) tests for cases where pier strengthening and foundation strengthening are implemented. In addition, analysis based on the PSD test algorithm is conducted to investigate the influence of pier strengthening on seismic damage to the foundation. The PSD-tests and the analysis show that the foundation suffers increased hysteretic response when pier strengthening is applied. The results also show that the foundation strengthening can prevent foundation damage.

KEYWORDS: pseudodynamic test, structure-foundation interaction, seismic strengthening

1. INTRODUCTION

In the 1995 Great Hanshin Earthquake (Kobe), the severe damage caused to many bridges mainly arose because their RC piers lacked sufficient load carrying capacity and ductility (Kawashima and Shigeki 1995). Consequently, many bridge piers in Japan have since been strengthened (Unjoh et al. 2000), using various techniques, so that they will withstand future strong earthquakes. Steel jacketing (Priestly et al. 1996 and Task group 2007), shown in Fig. 1(a), enhances the shear capacity and ductility of the pier without increasing flexural capacity. This is achieved by allowing space between the lower edge of the jacket and the footing, thereby avoiding flexural strength enhancement of the plastic hinge. However, in actual construction, flexural capacity may increase as a result of casting concrete with steel anchorages at the bottom of the pier. Another method of strengthening is by concrete jacketing (Priestly et al. 1996 and Task group 2007), shown in Fig. 1(b), which always enhances both the shear and flexural capacity of the pier. Also available is the method of externally bonding FRP sheet to the pier to enhance shear capacity and ductility (Priestly et al. 1996 and Task group 2007).

Enhancement of the load carrying capacity of a bridge pier by one of these techniques may influence the location and degree of seismic damage incurred when a strong earthquake occurs. In particular, it is anticipated that such strengthening may cause damage to be concentrated in the foundation. However, it is preferable that the damage should be easily investigated after an earthquake so that an appropriate judgment for restoration can be made. Consequently, a bridge should be designed as to avoid, as far as possible, any damage to its foundation. This means that strengthening of the foundation may also be necessary in some cases of seismic strengthening work. However, there have been very few studies on the seismic strengthening of bridge foundations.

In order to verify overall seismic behavior of a bridge system comprising superstructure, pier, and foundation, pseudo-dynamic (PSD) tests (Shing et al. 1996) are used. The PSD test, which combines merits of analysis and experiment, has evolved over the past 35 years from the original ramp-and-hold actuator control scheme (Takanashi and Nakashima et al. 1987) to, over the last decade, development of a real-time actuator control

algorithm (Nakashima et al. 1987, Pinto et al. 2004, and Jung et al. 2007). Using a sub-structuring technique (Dermitzakis et al. 1985), researchers can investigate the seismic response of the whole structural system by conducting experiments focusing on target members whose behavior is unclear. There were several interesting PSD tests conducted at ELSA laboratory in Italy (Pinto et al. 2004 and Pegon and Pinto 2000) for seismic assessment of bridges, but the presence of foundation was not considered. Toki et al. (1990) have utilized the PSD test to study the frequency-dependent dynamic characteristic of a foundation, but the interaction between pier and foundation was not included. Also, Kobayashi et al. (2002) introduced a sophisticated hybrid system utilizing a real-time actuator with a large shaking table attached to the base. However, such a system cannot be used extensively due to cost limitations.

The objectives of this paper are to 1) develop a PSD test system for evaluating overall seismic behavior of a bridge; 2) investigate foundation damage in bridges with pier strengthening; and 3) investigate the behavior of bridges with foundation strengthening.

2. SIMPLIFIED MODEL OF BRIDGE PIER SYSTEM FOR PSD TESTS

The behavior of a bridge subjected to ground acceleration is evaluated using a simplified three degrees of freedom (3-DOF) model as shown in Figure 2. This model is an extension of the single degree of freedom (SDOF) model used in the standard design method for a bridge pier (Japan Road Association 2002). Foundation movement is taken into account in terms of sway and rocking motions. The mass of the footing and the rotational inertia of the system are also included. Many researchers have used this sway and rocking model in modeling the seismic behavior of foundations (Mylonakis et al. 2006 and Ono et al. 2004), and it is also implemented as an alternative structural model in the design specifications of the Architectural Institute of Japan (Architectural Institute of Japan 1996). In this model, only three displacement components are considered: lateral displacement at pier top (u_1, m); lateral displacement at footing (u_2, m); and footing rotation (u_3, rad). The model also involves three inertial terms: the lump mass of the superstructure (m_1, kg); the lump mass of the footing (m_2, kg); and the rotational inertia (I, kg-m^2) of the system. The restoring force of the pier and the lateral and

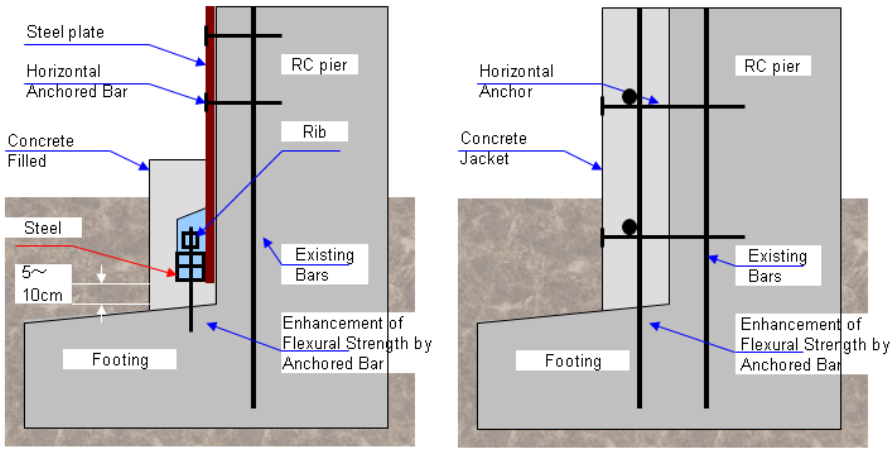

a) Steel Jacket with Controlled Increase in Flexural Capacity

b) Concrete Jacketing with Increase in Flexural Capacity

Figure 1 Strengthening of RC pier

Figure 2 Idealized structural model of bridge

rotational restoring forces of the foundation are represented by three springs, respectively: pier spring (R_p, N); sway spring (R_s, N); and rocking spring (R_r, N). The pier height in meters is denoted by H. The equation of motion for the system can be formulated as Eq. (1).

$$\begin{bmatrix} m_1 & 0 & 0 \\ 0 & m_2 & 0 \\ 0 & 0 & I \end{bmatrix} \begin{Bmatrix} \ddot{u}_1 \\ \ddot{u}_2 \\ \ddot{u}_3 \end{Bmatrix} + [C] \begin{Bmatrix} \dot{u}_1 \\ \dot{u}_2 \\ \dot{u}_3 \end{Bmatrix} + \begin{Bmatrix} R_1 \\ R_2 \\ R_3 \end{Bmatrix} = - \begin{bmatrix} m_1 & 0 & 0 \\ 0 & m_2 & 0 \\ 0 & 0 & I \end{bmatrix} \begin{Bmatrix} \ddot{u}_g \\ \ddot{u}_g \\ 0 \end{Bmatrix} \tag{1}$$

In which, [C] is the damping matrix and $\ddot{u}_g$ is the ground acceleration (m/s^2). The restoring force vector, {R} = {R_1 R_2 R_3}^{T} , is given here in the global-coordinate sense.

After initializing the dynamic terms relating to displacement, a solution is obtained for each time step by applying Newmark's integration scheme (average acceleration). Firstly, the displacement vector $\{\tilde{u}^{n+1}\}$ and the velocity vector $\{\tilde{\dot{u}}^{n+1}\}$ of the predictor step (in global coordinates) are calculated from Eq. (2) and Eq. (3) using the displacement vector $\{\tilde{u}^{n}\}$ and the velocity vector $\{\tilde{\dot{u}}^{n}\}$ from the previous step, and Δt is the interval time step in seconds (Combescure and Pegon 1997).

$$\begin{Bmatrix} \tilde{u}_1^{n+1} \\ \tilde{u}_2^{n+1} \\ \tilde{u}_3^{n+1} \end{Bmatrix} = \{\tilde{u}^{n+1}\} = \{u^n\} + \Delta t \{\dot{u}^n\} + \frac{\Delta t^2}{4} \{\ddot{u}^n\} \tag{2}$$

$$\begin{Bmatrix} \tilde{\dot{u}}_1^{n+1} \\ \tilde{\dot{u}}_2^{n+1} \\ \tilde{\dot{u}}_3^{n+1} \end{Bmatrix} = \{\tilde{\dot{u}}^{n+1}\} = \{\dot{u}^n\} + \frac{\Delta t}{2} \{\ddot{u}^n\} \tag{3}$$

This displacement of the predictor step $\{\tilde{u}_{global}^{n+1}\}$ is then mapped into the local coordinates $\{\tilde{u}_{local}^{n+1}\}$ of each restoring spring using a transformation matrix [T] given in Eq. (4). Next, the displacements in the local coordinates are applied to either a restoring force versus displacement model or a displacement-controlled test in order to evaluate the restoring force vector $\{\tilde{R}_{local}^{n+1}\}$ in the local coordinates (predictor step). The restoring force vector is then reversel-mapped back to the global coordinates $\{\tilde{R}_{global}^{n+1}\}$ using a contravariant relationship, Eq. (5). In this study, the restoring force of the pier spring was assumed to fit a bi-linear model, whereas the restoring forces of the sway and rocking springs are obtained from a displacement-controlled test on a foundation specimen.

$$\begin{Bmatrix} \tilde{u}_p^{n+1} \\ \tilde{u}_s^{n+1} \\ \tilde{u}_r^{n+1} \end{Bmatrix} = \begin{bmatrix} 1 & -1 & -\mathrm{H} \\ 0 & 1 & 0 \\ 0 & 0 & 1 \end{bmatrix} \begin{Bmatrix} \tilde{u}_1^{n+1} \\ \tilde{u}_2^{n+1} \\ \tilde{u}_3^{n+1} \end{Bmatrix}$$

$$\text{or} \quad \{\tilde{u}_{local}^{n+1}\} = [T] \{\tilde{u}_{global}^{n+1}\} \tag{4}$$

$$\{\tilde{R}_{global}^{n+1}\} = [T]^T \{\tilde{R}_{local}^{n+1}\} \tag{5}$$

To avoid iteration in the calculation, the restoring forces of the corrector step $\{R^{n+1}\}$ in Eq. (6) is approximated according to the operator splitting method (Nakashima et al. 1990), in which the difference between the restoring forces in the predictor step and the corrector step is assumed to vary linearly with a stiffness equals to the initial stiffness.

$$\{R^{n+1}\} = [KI]\{u^{n+1}\} + \{\tilde{R}^{n+1}\} - [KI]\{\tilde{u}^{n+1}\} \tag{6}$$

With the displacements $\{u^{n+1}\}$ and the velocities $\{\dot{u}^{n+1}\}$ of the corrector step as shown in Eq.(7) and Eq.(8), the acceleration vector $\{\ddot{u}^{n+1}\}$ is found to be the only unknown in Eq. (1), so this acceleration vector can be solved. The calculation can thus proceed to the next step.

$$\begin{Bmatrix} u_1^{n+1} \\ u_2^{n+1} \\ u_3^{n+1} \end{Bmatrix} = \{u^{n+1}\} = \{\tilde{u}^{n+1}\} + \frac{\Delta t^2}{4} \{\ddot{u}^{n+1}\} \tag{7}$$

$$\begin{Bmatrix} \dot{u}_1^{n+1} \\ \dot{u}_2^{n+1} \\ \dot{u}_3^{n+1} \end{Bmatrix} = \{\dot{u}^{n+1}\} = \{\tilde{\dot{u}}^{n+1}\} + \frac{\Delta t}{2} \{\ddot{u}^{n+1}\} \tag{8}$$

It should be noted that this 3-DOF model has a limitation in that only the inertial interactions can be taken into account. As a result, this system is applicable when the inertial interactions play a dominant role, which is valid in most cases of bridges subjected to strong ground accelerations (Meymand 1998).

3. EXPERIMENTAL SET UP

3.1 Target structure

Figure 3 shows the typical RC bridge used as a target structure in this study. This bridge was designed according to the 1971 specification for earthquake-resistant design of highway bridges (Japan Road Association 1971), which was the provision applied to the major number of bridges in

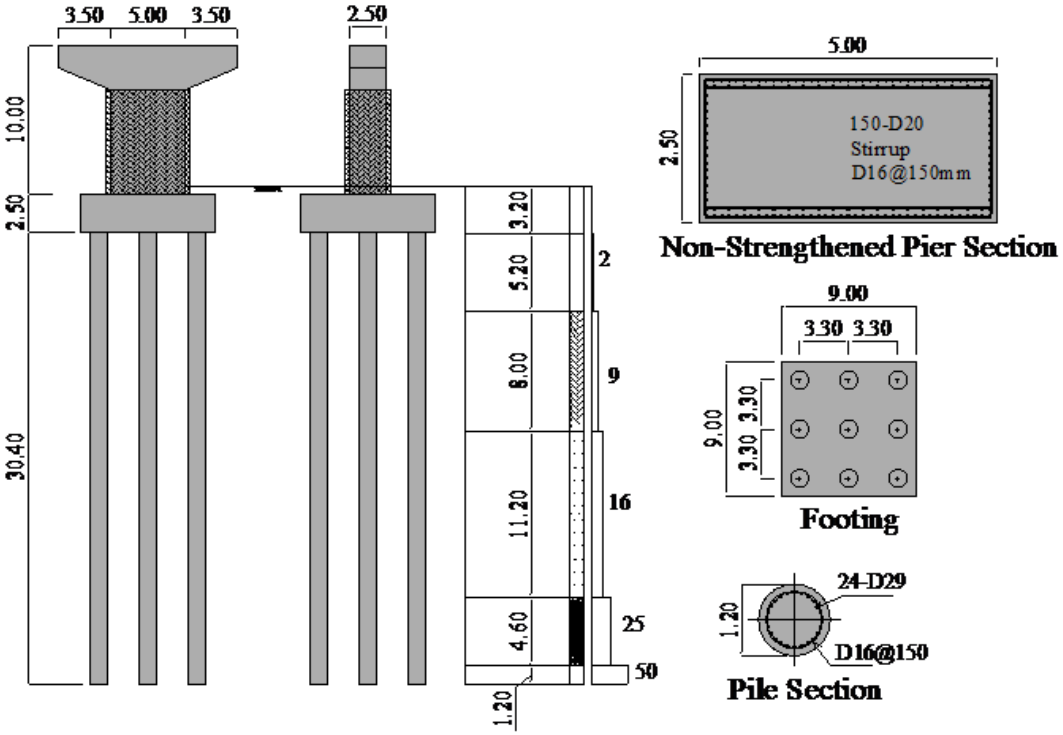

Figure 3. Target bridge structure

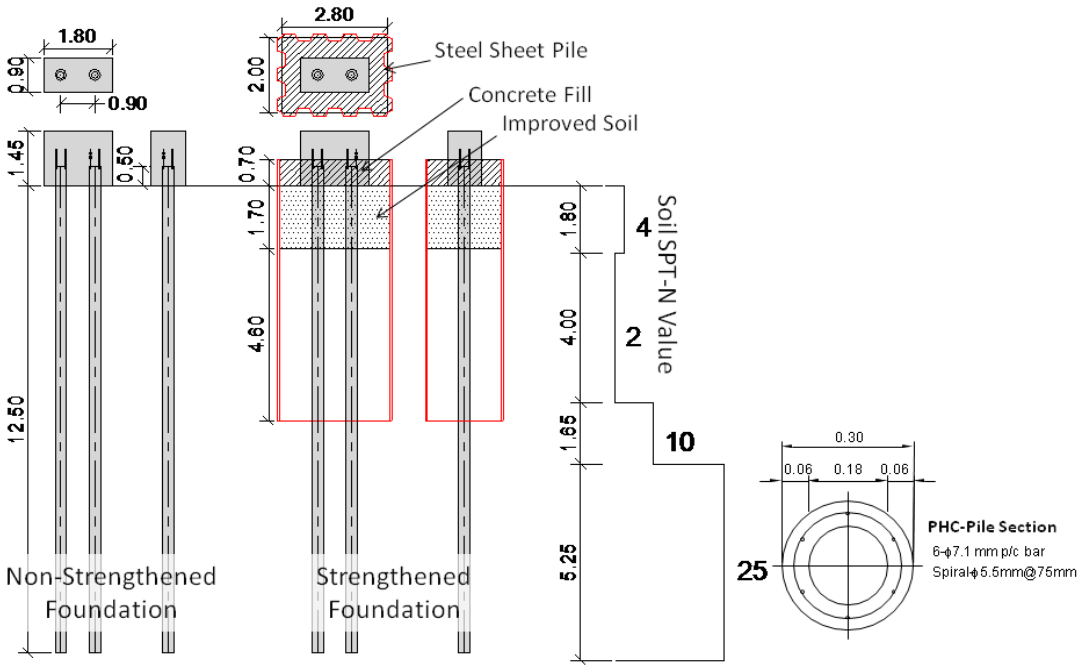

Figure 4 Foundation specimens for PSD-tests

Japan before the 1995 Great Hanshin Earthquake. The design lateral seismic force is 0.25 times the weight of the superstructure, adopting the allowable stress design method. Subsequently, the bridge pier was strengthened by the concrete jacketing technique with two times enhancement in flexural capacity.

3.2 Foundation specimen

PSD tests were carried out on two small-scale foundation specimens as shown in Figure 4. The first specimen is a non-strengthened foundation, while the second is the strengthened one. Two hollow-core prestressed high strength concrete (PHC) piles of 13.00 m length were installed under each foundation. The external diameter of each pile was 0.30 m and the hollow inside was of 0.18 m diameter. The concrete compressive strength was

79 MPa, and the yield stress of the prestressing bars was 1,275 MPa. Strain gages were attached along the prestressing bar inside the piles to investigate damage.

The piles were installed using the outside-drilling technique. In the installation process, the ground was first removed with an auger and then the drilled holes were stabilized by cement-bentonite slurry. The piles were then installed with their lower tips resting at -12.50 m in a sand stratum with a standard penetration value (SPT-N value) of 25. The full soil profile is also presented in Figure 4. The piles tops were anchored 0.50 m into the footing. The dimension of the footing was 0.90x1.80x1.45 m. In the case of the non-strengthened foundation, a gap of 0.03 m was provided in order to prevent friction between the footing and the ground.

The strengthening of the second specimen (Fukada et al. 2007) was carried out by installing steel sheet piles around the perimeter of the footing, maintaining a nominal clearance of 0.50 m. The sheet piles were of 7.00 m length, and were embedded -6.30 m into the ground. Their sections were 400 x 100 x 10.5 mm (width x depth x thickness). The ground enclosed by the sheet piles was removed and replaced by improved soil with a compressive strength of 1.8 MPa down to a depth of -1.75 m. Above the ground, the space between the footing and the sheet piles was filled up with concrete.

A bending test was conducted on a 7.00 m length pile with a similar cross section, with the results shown in Figure 5. The cracking curvature was 2.3×10^{-6} mm^{-1}. However, no clear yield point was observed. The failure mode was rupture of the prestressing bar at a corresponding ultimate curvature of 16.3×10^{-6} mm^{-1}.

Table 1 Estimated properties of target bridge

Inertial Properties			
Top Mass	1,080,000	Kg	
Footing Mass	486,000	Kg	
System Moment of Inertia	13,100,000	Kg-m^2	
Dimensional Properties			
Pier Section	2.50x5.00	m x m	
Pier Height	10.00	m	
Natural Period (sec)	Mode 1	Mode 2	Mode 3
Non-Strengthened Pier	0.66	0.19	0.08
Ratio	**1**	**: 0.28**	**: 0.12**
Design Stiffness Properties			
Pier (Bi-Linear Representation)	Yield Load (kN)	Yield Disp (m)	Stiffness (MN/m)
Non-Strengthened Pier	5,060	0.03	165.16
Sway	Ult. Load (kN)	Ult. Disp. (m)	Initial Stiffness (MN/m)
Normal Foundation	11,220	0066	415.35
Rocking	Ult. Mom. (kN-m)	Ult.Rot. (rad)	Initial Stiffness (MN-m)
Normal Foundation	172,920	0.006	68,591

Table 2 Estimated properties of scaled down bridge for PSD test

Inertial Properties				
	Top Mass	11,159	Kg	
	Footing Mass	5,022	Kg	
	System Moment of Inertia	3,912	Kg-m^2	
Dimensional Properties				
	Pier Section	0.23x0.46	m x m	
	Pier Height	0.94	m	
	Natural Period (sec)	Mode 1	Mode 2	Mode 3
	Non-Strengthened Pier	0.37	0.11	0.05
	Ratio	**1**	**: 0.28**	**: 0.13**
Design Stiffness Properties				
Pier (Bi-Linear representation)		Yield Load (kN)	Yield Disp (m)	Stiffness (MN/m)
	Non-Strengthened Pier	65.66	0.013	4.81
	Strengthened Pier	131.32	0.013	9.61
Sway		Ult. Load (kN)	Ult. Disp. (m)	Initial Stiffness (MN/m)
	Normal Foundation	125.85	0.034	12.950
	Strengthened Foundation	837.63	0.041	84.250
Rocking		Ult. Mom. (kN-m)	Ult.Rot. (rad)	Initial Stiffness (MN-m)
	Normal Foundation	301.27	0.01	64.52
	Strengthened Foundation	937.50	0.009	782.21

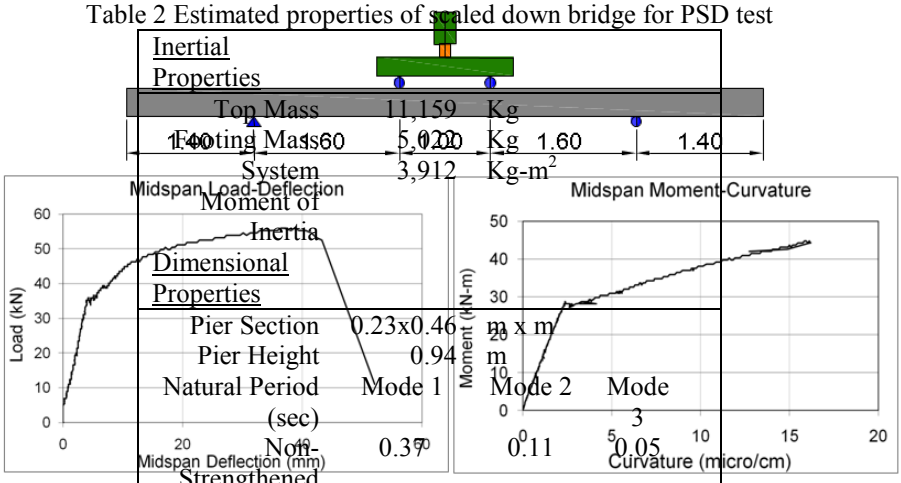

Figure 5. Pile bending test

3.3 Scaled down bridge for PSD test

The target bridge was scaled down for used in the PSD-tests such that the response spectrum remained similar. The scaling process was done based on the properties of the target bridge. All essential parameters of the target bridge were estimated based on the 3-DOF model, as displayed in Table 1. In addition, the three natural periods of the target bridge were calculated as well as the ratios between them. These ratios were used as key properties in the scaling process.

The ultimate loads and deformations of the non-strengthened foundation specimen were separately estimated for sway and rocking motions. The other parameters of the scaled-down bridge were then selected in order that the ratios of the three natural periods of the target bridge match those of the scaled-down bridge. As a result, parameters for the non-strengthened scaled-down bridge could be set up as shown in Table 2. Finally, the properties of the pier strengthening, also shown in Table 2, were determined assuming two times enhanced load carrying capacity and stiffness. In addition, the ultimate load and deformation of the strengthened foundation specimen were also estimated.

3.4 Input ground acceleration

The input ground acceleration is shown in Figure 6. Because of a limitation on experimental time, only 3.50 seconds (175 steps with 0.02 second incremental step) of ground acceleration were extracted from the Kobe record. The amplitude was scaled up to a peak ground acceleration of 1,182 gals to generate a large response. The response spectrum (5% damping) of this input ground acceleration is compared to the spectrum of the original wave in Figure 7, where the three natural periods of the corresponding bridges are also shown. The incremental time step was adjusted to 0.01 second in order to keep the positions of the three natural periods of the scaled-down bridge matched with those of the target bridge in relation to the response spectrum of the ground acceleration. With this response spectrum similarity, the scaled-down bridge can be used to represent the target one.

3.5 PSD test set up

The two PSD tests were carried out as follows:

Bridge-A: The scaled down bridge with pier strengthening sited on a non-strengthened foundation

Bridge-B: The scaled down bridge with pier strengthening sited on a strengthened foundation.

3.5.1 PSD test set up for Bridge-A

The PSD test was carried out according to the algorithm discussed in section 2. The input mass terms for the 3-DOF model were those of the scaled-down bridge in Table 2. The load-deformation relationship of the strengthened pier was idealized using the bi-linear model shown in Figure 8(a). The bi-linear model parameters are given in Table 3.

Table 3. Parameters of bi-linear model for piers

Pier	PY (kN)	YY (m)	a	b
Non-Strengthened	65.66	0.013	0.0	0.1
Strengthened	131.321	0.013	0.0	0.1

In order to obtain the load-deformation responses of the foundation, an experiment was conducted on the non-strengthened foundation specimen with a configuration shown in Figure 9(a). Two hydraulic jacks were utilized to simultaneously apply both sway and rocking displacements to the specimen. The lower jack was placed 0.38 m above the ground, which is the assumed level of the footing centroid, and the upper one was installed 0.75 m higher. This configuration made it possible to include the interaction of sway and rocking motions in the test.

3.5.2 PSD test set up for Bridge-B

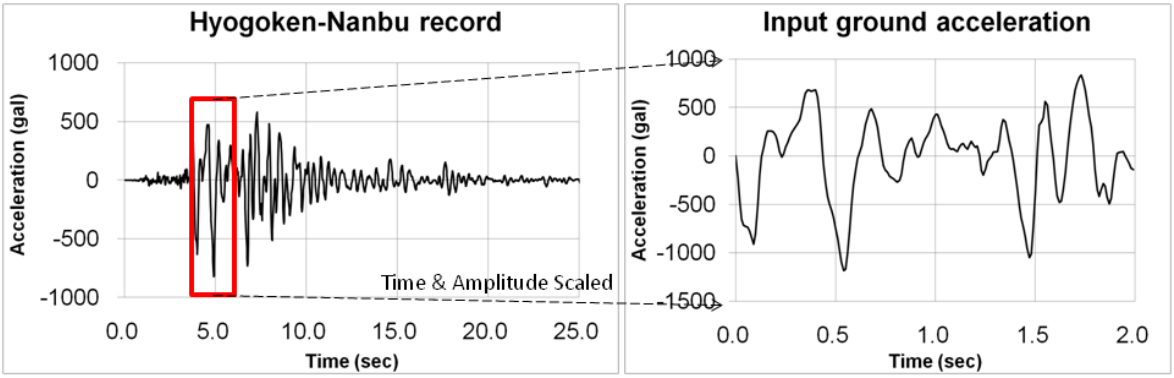

Figure 6. Input ground acceleration

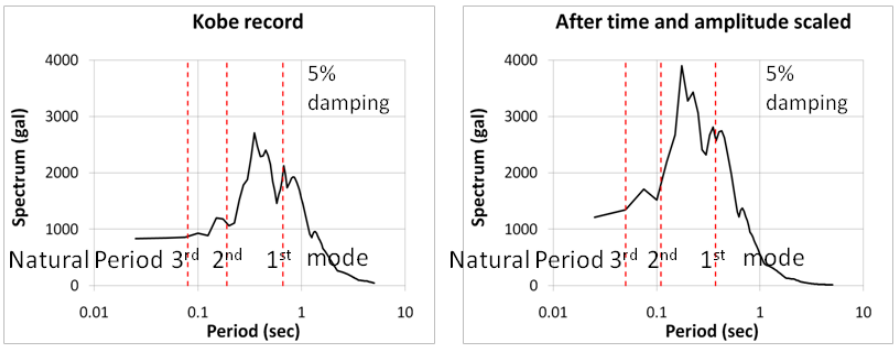

Figure 7 Response spectrum of original acceleration and scaled version

The mass terms and the bi-linear parameters for the strengthened pier were the same as those used for Bridge-A. The experiment was carried out on the strengthened foundation specimen to obtain the load-deformation responses of the foundation. In this experiment, sway displacements only were applied to the specimen using the lower jack, as shown in Figure 9(b). In parallel, a linear model was assigned to the load-deformation relationship for rocking motion using the estimated rocking stiffness of the strengthened foundation given in Table 2. Since the strengthened foundation possesses a high rotational rigidity as well as capacity, interaction between sway and rocking movement is negligible. This configuration, in turn, vastly simplifies the experimental set up. It should be noted that Rayleigh's damping of 5% was applied in these two PSD tests.

4. RESULTS AND DISCUSSIONS

The results of the PSD-tests are presented in Figure 10. In the case of Bridge-A, the pier response has just reached the yield point with a ductility of 1.01. On the other hand, a clear reduction in stiffness slope could be observed in the sway load-deformation response of the foundation. After the PSD test, the ultimate loading capacity of the specimen was checked by increasing the lower jack force towards failure in both directions. This result is included in the sway response of Bridge-A in Figure 10. The peak sway deformation of the foundation during the PSD test was 83% of the observed ultimate displacement, while the overall ductility capacity of the foundation was about 6. There is no clear sign of yielding in the rocking response of Bridge-A.

In contrast, the PSD test on Bridge-B gives a ductility of 4.04 for the pier, whereas the sway motion of the foundation is an almost linear response with little deformation. A small response is also observed in the rocking motion.

The maximum curvature in the piles, calculated from the measured strain data, is shown in Figure 11. In the case of Bridge-A, the observed maximum curvatures on the left and right hand sides were 11.4×10^{-6} mm^{-1} and 24.9×10^{-6} mm^{-1}, respectively. Remarkably, the maximum curvature of the right hand pile is greater than the ultimate curvature of 16.3×10^{-6} mm^{-1} observed in the bending test. In contrast, Bridge-B exhibits very little curvatures in its two piles.

The PSD-test results for Bridge-A show that damage is concentrated in the foundation. This contradicts the seismic design strategy, according to which damage is expected to concentrate in the pier as this should be the energy-dissipation member. Allowing such foundation damage may be inappropriate in light of the difficulty regarding damage investigation as well as restoration after an earthquake. On the other hand, the PSD test results for Bridge-B clearly indicate the ability of foundation strengthening to prevent foundation damage.

5. ANALYSIS BASED ON PSD TEST ALGORITHMS

A series of analyses were carried out based on the PSD test algorithm in order to:

1. compare the seismic behavior of the bridge before and after pier strengthening
2. compare the seismic behavior of the bridge after foundation strengthening with its behavior in the design using the fixed base model

make clear changes in damage location in the strengthened bridge using various pier and foundation configurations.

5.1 Seismic behavior of bridge before pier strengthening

The 3-DOF model for the PSD tests was used as the idealized structural model in this analysis, again using the same mass terms as given in Table 2. The bi-linear model in Figure 8(a) was assigned to the load-deformation relationship of the pier with the parameters given for the non-strengthened pier in Table 3. The sway load-deformation relationship of the foundation employed the bi-linear model shown in Figure 8(b), whereas a linear model was assigned to the rocking motion. The model parameters for the non-strengthened foundation, given in Table 4, were determined

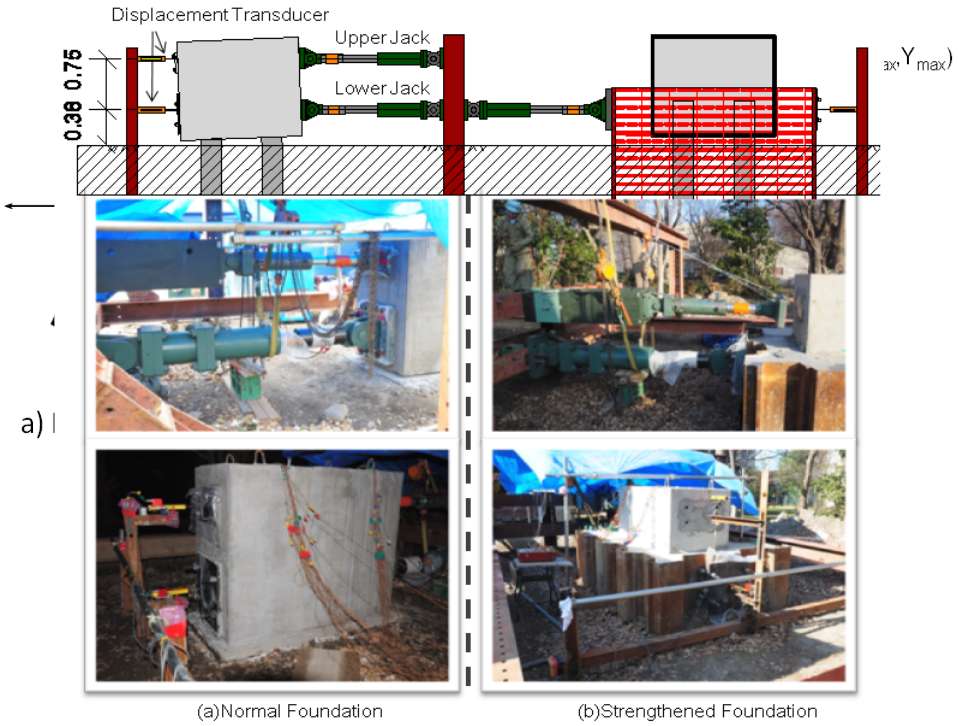

Figure 9 PSD test set up

based on the PSD test results for Bridge-A, and were verified by conducting an analysis of Bridge-A. The analytical results for Bridge-A are included in Figure10 for comparison with those of the PSD test. There is a good agreement between the two.

The load-deformation responses of the non-strengthened pier are compared with those of the strengthened pier in Figure 12. The maximum ductility of the non-strengthened pier is 5.75, while that of the strengthened one is reduced to 1.15. In contrast, the maximum ductility in foundation sway motion is 1.02 in the case of the non-strengthened pier, while it is 8.69 in the strengthened pier. Similarly, an increase in rocking response is also observed.

The results for the non-strengthened pier show that the damage is concentrated in the pier. In other words, this confirms that the location of damage shifts into the foundation as a result of pier strengthening.

5.2 Seismic behavior of bridge with foundation strengthening compared to fixed-base pier

An analysis of the Bridge-B was conducted using linear load-deformation relationships for both sway and rocking motions of the foundation. The stiffness of these linear models, as given in Table 4 (for the strengthened foundation), was determined based on the PSD test results of Bridge-B. The results of this analysis are included in Figure 10 for comparison with the corresponding PSD test.

Another analysis was then conducted using the SDOF (fixed base) model shown on the left-hand side of Figure 2. It should be noted that only the top mass and the bi-linear model of the strengthened pier were involved in this analysis. The acceleration at the pier top and the load-deformation response of the pier in the SDOF model are compared with the earlier analysis of Bridge-B in Figure 13. There is a good agreement of the response behavior between the SDOF model and Bridge-B. It may be concluded that if foundation strengthening provides sufficient stiffness and capacity, the seismic interaction of the foundation may reduced to a negligible amount since a foundation of greater stiffness and capacity approximates a fixed base.

5.3 Seismic behavior of bridges with various pier and foundation capacities

Based on the analytical model of the non-strengthened foundation described in Table 4, a series of analyses were conducted with various pier and foundation capacities as to clarify how the location of damage shifts in the bridge pier and foundation system.

5.3.1 Seismic behavior of bridges with increasing pier capacity

Analyses were carried out based on the PSD test algorithm. The model parameters for the non-strengthened foundation given in Table 4 were used. On the other hand, the bi-linear model for the pier was varied, with yield loads equivalent to 50%, 60%, 70%, etc. up to 200% of the sway motion of the foundation. Two series of analyses were carried out with different pier yield displacements, as follows:

Series A: The stiffness of the piers with different capacities was maintained equal to the

stiffness of the non-strengthened pier. As a result, the yield displacements of the piers were also varied according to their corresponding yield loads. This was intended to constrain the change in natural frequency, thereby suppressing the effect of frequency-dependent response.

Series B: The yield displacements of the pier were equal to the yield displacement of the non-strengthened pier.

For Series A, the ductility of the pier and the sway motion of the foundation are plotted against the ratios of pier yield load to sway motion in Figure 14(a). It is noteworthy that an increasing ratio of the two yield loads (the x-axis) corresponds to increasing pier capacity. Pier ductility is higher than that of the sway motion for lower values of the ratio between the two yield loads. This implies that damage takes place in the pier when the capacity of the pier is low. With increasing pier capacity, damage gradually shifts down into the foundation as pier ductility falls, while sway ductility increases. The ductility of the pier and the sway motion then intersect when the ratio of their yield loads is about 0.8. In this configuration, both pier and foundation may suffer damaged, as both ductilities are about 4. After this point, with the ductility of the sway motion greater than that of the pier, damage moves to the foundation. Sway ductility ultimately converges to a constant value if pier does not yield (pier ductility < 1).

The results for Series-B are shown in Figure 14(b). The trends in pier ductility and sway ductility are similar to those observed with Series-A. In this case, ductility changes more abruptly with varying pier capacity. In addition, the ductility of the sway motion, instead of becoming a constant value, infinitesimally drops after no yielding occurs in the pier. These results arise because frequency-dependent responses also participate.

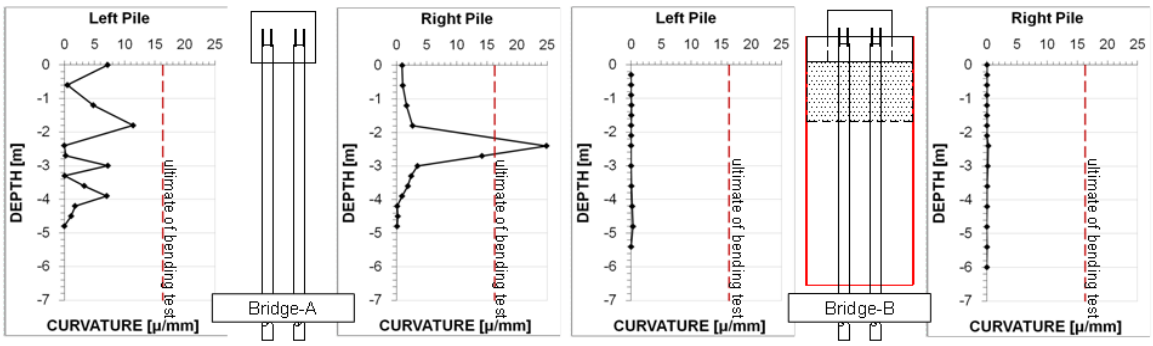

Figure 11 Curvature distribution in piles

5.3.2 Seismic behavior of bridges with increasing foundation capacity

The effect of increasing foundation capacity on the seismic behavior of a bridge is discussed through analyses using four pier configurations sited on foundations with varying capacities. The yield loads of the four piers were respectively 100%, 133%, 167% and 200% that of the non-strengthened pier (Table 3). On the other hand, the yield loads of sway motion in the foundations were 60%, 80%, 100%, etc. up to 340% that of the non-strengthened foundation. The stiffness of the pier and the sway motion of foundation were kept equal to those of the non-strengthened pier and the non-strengthened foundation, respectively. The linear model for the rocking motion of the non-strengthened foundation was used throughout this analysis.

The results are given in Figure 15, in which Figure 15(a) shows the maximum pier ductility with varying foundation yield load (sway motion).

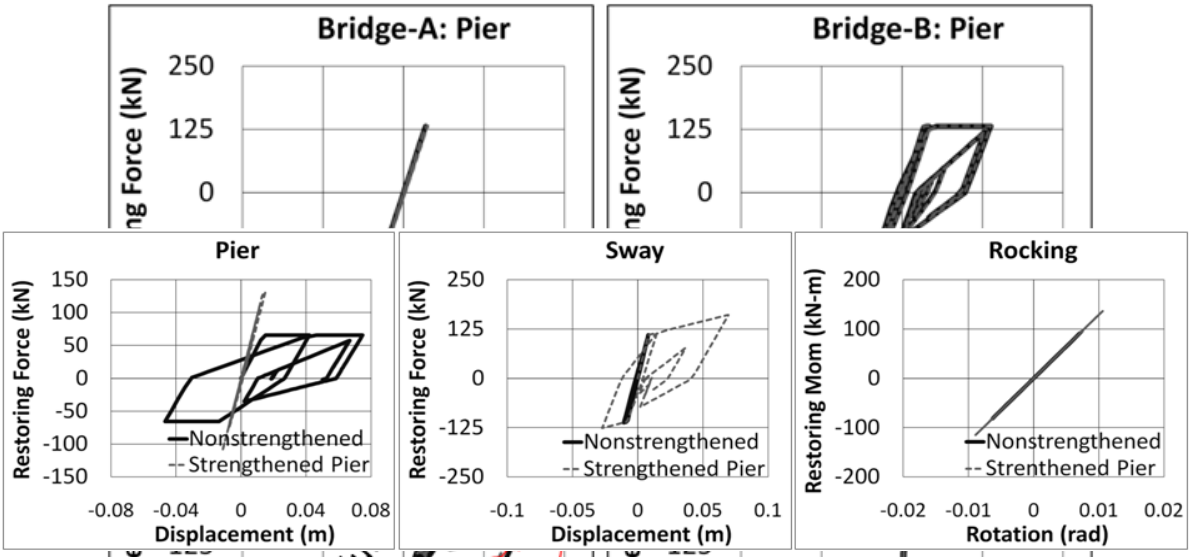

Figure 12 Analysis of non-strengthened and pier-strengthened bridge

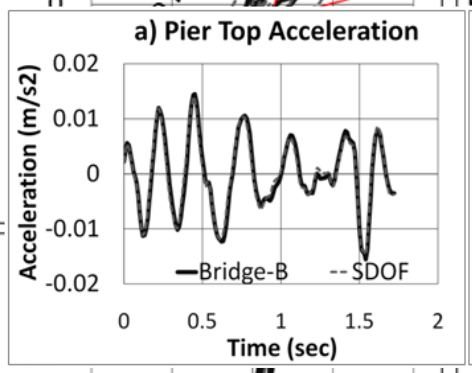

Figure 13 Comparison between pier response of Bridge-B and SDOF model

Figure 10 PSD test results

The ductility of the four piers increases with increasing foundation yield load with each ultimately converging to a constant value with high foundation yield load. The stronger the pier capacity, the smaller the bounded value of pier ductility was observed. On the other hand, Figure 15(b) shows the maximum load in the foundation against the foundation yield load. The dotted line in the graph presents an equality of the maximum load in the foundation and the foundation yield load. In the area above this line, yielding of the foundation occurs, whereas the foundation does not yield in the area underneath. For all piers, the maximum load in the foundation increases with increasing foundation yield load, and then stop

Found

b

Nc

Streng

0.4

Streng

-

-

-

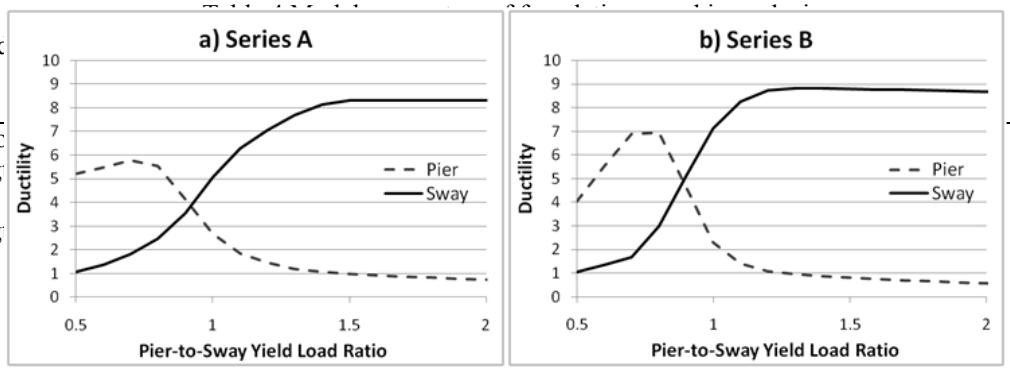

Figure 14 Ductility of pier and foundation (sway) with varying pier capacity

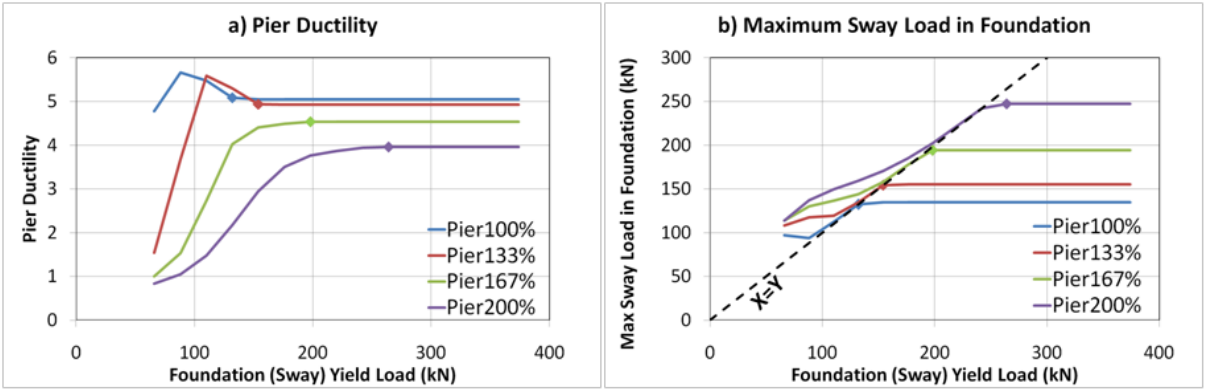

Figure 15 Seismic behavior of bridge with increasing foundation capacity

suddenly at a constant value once the dotted line into the no yielding range is crossed. It is also of interest that pier ductility in Figure 15(a) also reaches a bound at which its value becomes constant since the maximum load in the corresponding foundations crosses the dotted line into the no yielding range. This transition is marked by a dot on each curve, representing the corresponding configurations in Figure 15(a) and Figure 15(b).

From these results, it is clear that, as foundation capacity increases, the behavior of a bridge tends to be bound with respect to both the pier ductility and maximum load in the foundation. If the change in natural frequency is constrained, the response begins to converge on the bounded value soon after no yielding in the foundation is guaranteed. This condition, in fact, may be used as a reference point for a safety evaluation of the foundation as well as to determine the minimum requirement for foundation strengthening. Although, changing the stiffness of the pier and the foundation may alter these bounding values because of the involvement of frequency dependency, this frequency-dependent response may be negligible in a design where code specified ground accelerations are used in which their response spectra are held mostly constant over the range of significant natural periods.

6. CONCLUSION

In this study, the PSD tests for seismic performance evaluation of bridge pier and foundation has been proposed and implemented to investigate seismic behavior of bridges with pier strengthening and foundation strengthening. Additional analysis was also carried out to clarify how damage shifts between the pier and the foundation with different levels of strengthening. From the PSD tests and analysis, the following conclusions can be drawn:

1. As pier flexural capacity is enhanced through pier strengthening, the damage caused by future earthquakes may be concentrated in the foundation. If such damage occurs, post-earthquake investigation and repair are expected to be difficult.
2. The PSD-test on a strengthened foundation verified that foundation strengthening can effectively prevent the foundation damage which may occur after pier strengthening.
3. As foundation capacity is increased, bridges exhibit behavior with a bounding tendency. The maximum load in the foundation converges to a bounded value soon after no foundation yielding is ensured. This state can be used as the minimum required capacity for foundation strengthening.

REFERENCES

Architectural Institute of Japan, *Recommendations for Loads on Buildings*. Japan, 1996.

Combescure D, Pegon P. α-operator splitting time integration technique for pseudodynamic testing-error propagation analysis. *Soil Dynamics and Earthquake Engineering*, 1997; 16: 427-443.

Dermitzakis SN, Stavros N, Mahin SA. Development of substructuring techniques for on-line computer controlled seismic performance testing. *UCB/EERC-85/04*, Earthquake Engineering Research Center: Berkeley, 1985.

Fukada H, Kato K, Segawa N, Ooya T and Shioi Y. A study of reinforcement methods for existing bridges on soft ground with a solidification improvement. *Advanced in Deep Foundations*, Taylor & Francis Group, London, 2007.

Japan Road Association, *Specifications for highway bridges*. Japan, 2002.

Japan Road Association, *Specifications for highway bridges*. Japan, 1971. (in Japanese).

Jung RY, Shing PB, Stauffer E and Thoen B. Performance of a real-time pseudo-dynamic test system considering non-linear structural response. *Earthquake Engineering and Structural Dynamics* 2007; 36:1785-1809.

Kawashima K, Shigeki U. Impact of Hanshin/Awaji earthquake on seismic design and seismic strengthening of highway bridges. *1995 Hyogoken-nanbu earthquake*, Committee of Earthquake Engineering – Japan Society of Civil Engineers, June, 1996.

Kobayashi H, Tamura K, Tanimoto S, Hybrid vibration experiments with a bridge foundation system model. *Soil Dynamics and Earthquake Engineering* 2002; 22:1135-1141.

Meymand PJ, 'Shaking table scale model test of non-linear soil-pile-superstructure interaction in soft clay', *Ph.D. Dissertation*, University of California, Berkeley, 1998.

Unjoh S, Terayama T, Adachi Y and Hishikuma J. Seismic retrofit of existing highway bridges in Japan. Cement and concrete composites 2000; 22(1):1-16.

Mylonakis G, Nikolaou S and Gazetas G. Footing under seismic loading: analysis and design issues with emphasis on bridge foundations. *Soil Dynamics and Earthquake Engineering* 2006; 26:824-853.

Nakashima M, Kaminosono T, Ishida M, Ando K. Integration Technique for Substructure Pseudo Dynamic Test. *Proc. of the 4th U.S. National Conference on Earthquake Engineering*, 1990; 2:515-524.

Nakashima N, Kato H, Takaoka E. Development of real-time pseudo dynamic testing. *Earthquake Engineering and Structural Dynamics* 1992; 21:79-92.

Ono Y, Kiyono J, Toki K. Effects of pile-foundation-soil interaction on demanded strength of highway bridge pier. *Proc. of the 13th World Conference on Earthquake Engineering*, Paper no. 168, Vancouver, Canada, 2004.

Pegon P, Pinto AV. Pseudo-dynamic testing with substructuring at the ELSA laboratory. *Earthquake Engineering and Structural Dynamics* 2000; 29:905-925.

Pinto AV, Pegon P, Magonette G and Tsionis G. Pseudo-dynamic testing of bridges using non-linear substructuring. *Earthquake Engineering and Structural Dynamics* 2004; 33:1125-1146.

Priestly NMJ, Seible F and Calvi M. *Seismic Design and Retrofit of Bridges*. John Wiley & Sons: New York, 1996.

Shing PB, Nakashima M, Bursi OS. Application of pseudodynamic test method to structural research. Earthquake Spectra 1996; 12(1):29-56.

Takanashi K, Nakashima M. Japanese activities on on-Line testing. *Journal of Engineering Mechanics* (ASCE) 1987; 113(7):1014-1032.

Task Group 7.4 – International Federation for Structural Concrete (fib) (Bullentin 39), *Seismic bridge design and retrofit – structural solutions*. Sprint-Digital-Druck: Stuttgart, 2007.

Toki K, Sato T, Kiyono J, Garmroudi N K, Emi S, Yoshikawa M, Hybrid experiments on non-linear earthquake-induced soil-structure interaction. *Earthquake Engineering & Structural Dynamics* 1990; 19:709-723.